A global analysis of reconstructed land climate changes during Dansgaard-Oeschger events

Mengmeng Liu[1,2,*], Iain Colin Prentice[1], Sandy P. Harrison[2]

1: Georgina Mace Centre for the Living Planet, Department of Life Sciences, Imperial College London, Silwood Park Campus, Buckhurst Road, Ascot SL5 7PY, UK

2: Department of Geography and Environmental Science, University of Reading, Reading, RG6 6AB, UK

*** Corresponding author: m.liu18@imperial.ac.uk**

Ms for: *Climate of the Past*

Abstract

Dansgaard–Oeschger (D–O) warming events are comparable in magnitude and rate to the anticipated 21st century warming. As such, they provide a good target for evaluation of the ability of state-of-the-art climate models to simulate rapid climate changes. Despite the wealth of qualitative information about climate changes during the D-O events, there has been no attempt to date to make quantitative reconstructions globally. Here we provide reconstructions of seasonal temperature changes and changes in plant-available moisture across multiple D-O events during Marine Isotope Stage 3 based on available pollen records across the globe. These reconstructions show that the largest warming occurred in northern extratropics, especially Eurasia, while western North America and the southern extratropics were characterised by cooling. The change in winter temperature was significantly larger than the change in summer temperature in the northern extratropics, indicating that the D-O warming events were characterised by reduced seasonality, but there is no significant difference between the summer and winter temperature changes in the southern extratropics and the tropics. The antiphasing between northern and southern extratropical changes, and the west-east pattern of cooling and warming in North America are consistent across the eight D-O events examined, although the signal at individual sites may vary between events. Globally, changes in moisture were positively correlated with changes in temperature, but the strength and the sign of this relationship vary regionally. These reconstructions can be used to evaluate the spatial patterns

29 of changes in temperature and moisture in the transient simulations of the D-O events planned
30 as part of the Palaeoclimate Modelling Intercomparison Project.

1. Introduction

Dansgaard–Oeschger (D–O) events are characterised in Greenland by a transition from cold Greenland Stadial (GS) to warmer Greenland Interstadial (GI) conditions (Dansgaard et al., 1993). The surface air temperature in Greenland increased by 10–15° C during the warming phases; these warming events occur over an interval of between 50 and 200 years (Huber et al., 2006; Kindler et al., 2014). Thus, the D-O events offer a parallel in terms of speed to projected future warming, although both the baseline state and the mechanism inducing this warming differ from anticipated 21st century climate changes. D-O events could therefore provide an opportunity to determine how well climate models that are used for future projections can simulate rapid climate changes (Malmierca-Vallet et al., 2023), particularly regional patterns of warming (and cooling) that are regarded as a challenge for modelling (Doblas-Reyes et al., 2021; Lee et al., 2021) and are highly important in assessing the vulnerability of human societies to future climate changes (IPCC 2022).

D-O events are registered globally (Voelker, 2002; Sánchez Goñi and Harrison, 2010; Harrison and Sánchez Goñi, 2010; Sánchez Goñi et al., 2017; Adolphi et al., 2019; Corrick et al., 2020). Shifts in vegetation types between GI and GS states have been interpreted as primarily a temperature signal in the extratropics and a moisture signal in the tropics (Harrison and Sánchez Goñi, 2010). Speleothem records provide a good time-control on the synchroneity of climate changes globally with the D-O events registered in Greenland (Adolphi et al., 2019; Corrick et al., 2020), but the driver of this signal can either be temperature or precipitation depending on the region. There are quantitative climate reconstructions based on terrestrial pollen records from La Grande Pile (Guiot et al., 1993), Lago Grande di Monticchio (Huntley et al., 1999), Padul (Camuera et al., 2022), El Cañizar de Villarquemado (Wei et al., 2021; Camuera et al., 2022) and Lake Ohrid (Sinopoli et al., 2019), marine cores in the western Mediterranean and offshore from Portugal (Sánchez-Goñi et al., 2002), diatom assemblages at Les Echets, France (Ampel et al., 2010), bacterial membrane lipid records from the Eifel region (Zander et al.,2023), isotopic measurements of earthworm calcite from the Rhine Valley (Prud'homme et al., 2022) and clumped isotope measurements on snails in Hungary (Újvári et al., 2021). Aside from the lack of comparable quantitative estimates from outside Europe, differences in the methodology employed and in the specific climate variables reconstructed in each of these studies limits their usefulness for model evaluation. In particular, given that there is still uncertainty as to whether the D-O cycles are characterised by changes in seasonality

such that warming events are primarily driven by changes in winter (Flückiger et al., 2008; Zander et al., 2024), in the regional strength of the warming (Harrison and Sánchez Goñi, 2010) and how warming relates to changes in moisture (Wei et al., 2021), there is a need for more systematic reconstruction of seasonal climate changes.

In the paper, we provide reconstructions of seasonal temperature changes and changes in plant-available moisture during the intervals corresponding to D-O warming events in Greenland during Marine Isotope Stage 3 based on available pollen records globally. We employ a standard methodology to construct age models for these records, as well as a standard regression-based approach to make the reconstructions. We analyse the regional patterns to identify key targets for model evaluation.

2. Methods

2.1. Data sources

Modern pollen data were obtained from version 2 of the SPECIAL Modern Pollen Data Set (SMPDSv2: Villegas-Diaz and Harrison, 2022). This global data set contains 24649 modern pollen records from 17827 sites. The dataset contains relative abundance records for 4816 pollen taxa, created after removing taxa that are not climatically diagnostic (e.g. obligate aquatics, carnivorous species, cultivated plants). The data set provides several levels of taxonomic aggregation; here we use the most aggregated level, where woody species were generally combined at genus level and herbaceous species at sub-family or family level unless they were palynologically distinctive, occupied distinctive ecological niches and were sufficiently geographically widespread. This "amalgamated" data set contains relative abundance information for 1338 taxa. These samples were aggregated by longitude, latitude and elevation in order to remove duplicates. Counts for *Quercus*, *Quercus* (deciduous) and *Quercus* (evergreen) were combined because of inconsistent differentiation of *Quercus* pollen in different regional records. Deciduous and evergreen oaks occupy different areas of climate space, particularly in terms of seasonal moisture; specifically, evergreen oaks are typically found in areas characterised by winter rainfall such as the Mediterranean. Nevertheless, since there are other plant taxa that are similarly diagnostic of such regimes, the amalgamation of *Quercus* (deciduous) and *Quercus* (evergreen) should not have a major effect on the robustness of our climate reconstructions. Taxa that occurred in less than 10 samples in the training data set were not used to make reconstructions because it is unlikely that the available samples

provided a reasonable estimate of the climate space occupied by these rare taxa (Liu et al., 2020). After filtering, the data set contains information on 591 individual pollen taxa from 17547 sites (Figure 1).

The SMPDSv2 also provides climatic information at each pollen site, specifically the mean temperature of the coldest month (MTCO), mean temperature of the warmest month (MTWA), and a plant-available moisture (α) calculated as the ratio of actual evapotranspiration to equilibrium evapotranspiration. α is a transformation of the commonly used moisture index MI, to emphasize the differences at the dry end of the climate range, which have a more pronounced effect on vegetation distribution than differences at the wet end (Prentice et al., 2017). Detailed relationships are in Supplementary Materials. These bioclimate variables reflect mechanistically distinct controls on plant growth.

The fossil pollen data were obtained from the Abrupt Climate Changes and Environmental Responses (ACER) database (Sánchez Goñi et al., 2017), which includes 93 records from the last glacial period (73-15 ka) with sufficient resolution and dating control to detect sub-millennial scale variability. Here we focus on the 73 records covering most of Marine Isotope Stage 3 (50-30 ka); 54 of these records are from terrestrial sites and 19 from marine sites (Figure 1; Table 1). The fossil data were taxonomically harmonised to be consistent with the SMPDSv2.

We have used a global pollen data set for calibration of the pollen-climate relationships, SMPDsv2 (Villegas-Diaz and Harrison, 2022). The use of a global data set, rather than region-specific training data, relies on the principle of phylogenetic niche conservatism (Harvey and Pagel, 1991), which states that traits tend to remain constant over time. This also applies to the climate niche (Wiens and Graham, 2005; Wiens et al., 2010; Peterson, 2011; Crisp and Cook, 2012; Jiang et al., 2023) as evidenced by disjunct distributions of taxa across different continents (Yin et al., 2021). Niche conservatism underpins the fact that the modern distribution of specific genera can be predicted using climate-pollen relationships developed from other regions (e.g. Huntley et al., 1989). The use of a global data set for calibration makes it possible to sample a large range of climates, and thus makes it more likely that the reconstructions of glacial climates are realistic and not confined to the limited climate range sampled in any one region (Turner et al., 2020). Indeed, Turner et al. (2020) have shown that increasing the size of the calibration data set tends to lead to smaller reconstruction errors and

more accurate estimates of taxon coefficients. Pragmatically, the use of a global data set also facilitates making reconstructions for sites from regions where there is limited modern pollen data.

2.2. Climate reconstruction method

We used tolerance-weighted Weighted Averaging Partial Least Squares (*fx*TWA-PLS: Liu et al., 2020; Liu et al., 2023) regression to model the relationships between taxon abundances and individual climate variables in the SMPDSv2 modern training dataset and then applied these relationships to reconstruct past climate using the fossil assemblages from the ACER database (Figure 2). *fx*TWA-PLS reduces the tendency of regression methods to compress reconstructions towards the centre of the sampled climate range by applying a sampling frequency correction to reduce the influence of uneven sampling of climate space and weighting the contribution of individual taxa according to their climate tolerances (Liu et al., 2020). Version 2 of *fx*TWA-PLS (*fx*TWA-PLS2, Liu et al., 2023) uses P-splines smoothing to derive the frequency correction and applies this correction both in estimating the climate optima and tolerances, and in the regression itself, producing a further improvement in model performance compared to version 1 (Liu et al., 2020).

We evaluated the *fx*TWA-PLS models by comparing the reconstructions with observations using leave-out cross-validation, where one site at a time was randomly selected as a test site and sites that are both geographically close (within 50 km horizontal distance from the site) and climatically close (within 2% of the full range of each climate variable in the dataset) were removed from the training set along with this test site, to prevent redundancy in the climate information from inflating the cross-validation goodness of fit, following Liu et al. (2020). We selected the last significant number of components (p-value ≤ 0.01) and assessed model performance using the root mean square error of prediction (RMSEP). Compression was assessed using linear regression of the leave-out cross-validated reconstructions on to the climate variable. Reconstructions of MTCO, MTWA and α were made for every sample in each fossil record. Sample specific errors were estimated via bootstrapping, as described in Liu et al. (2020). We corrected for the effect of changes in atmospheric CO_2 on plant water-use efficiency, and hence the reconstructions of α (Figure S1), following Prentice et al. (2022). Appropriate values of CO_2 were taken from the WAIS Divide ice core record (Bauska et al., 2021).

2.3. Age modelling

Although the ACER database provides age models for each pollen record, the resolution of the individual records is variable (mean resolution 474 years) and these models are often imperfectly aligned with the dating of D-O events as recorded in the Greenland ice core, and which have been shown to have a globally synchronous imprint through analysis of speleothem records (Adolphi et al., 2019; Corrick et al., 2020). To create a better alignment, we used dynamic time warping (DTW: Belman and Kalaba, 1959; Burstyn et al., 2021) to adjust the age scale for each individual record (Figure 2). Dynamic time warping optimises the similarity between two sequences by stretching or compressing one sequence in the time dimension to match the other. Here, we use simulated mean annual temperature (MAT) from a transient simulation of the interval 50-30 ka made with the LOVECLIM model (Menviel et al., 2014) as the reference sequence compared to MAT calculated as the average of MTCO and MTWA from the individual pollen records. We used the mid-point between the start dates of each D-O event (Wolff et al., 2010; converted into AICC2012 timescale) to sub-divide each ACER record into discrete intervals and modified the time scale of the reconstructed mean annual temperature series in each interval to match the reference sequence, having normalised both sequences to remove the influence of differences in absolute values and the amplitude of changes. The adjusted age model for each ACER record was then applied to the reconstructions of MTCO, MTWA, and α from that record for subsequent analyses.

2.4. Assessment of regional climate changes during Greenland D-O warming events

The magnitude of climate change during the interval corresponding to each D-O warming event as registered in Greenland is calculated individually for each climate variable at each site. To avoid making an assumption about the sign of the climate change at a site, we used a third-order polynomial to fit the reconstructions during the interval from 300 years before to 600 years after the official start date corresponding to Greenland D-O warming for each event (Wolff et al., 2010; converted into AICC2012 timescale) to determine whether the change was positive or negative. We used the ages corresponding to the minimum and maximum in the fitted polynomial ($t_{\text{min polynomial}}$, $t_{\text{max polynomial}}$) but restrict $t_{\text{min polynomial}}$ and $t_{\text{max polynomial}}$ to be found at where there are reconstructions. Since the smoothed polynomial may underestimate or overestimate the amplitude of change, we used the reconstructed minimum or maximum value

within the period $t_{min\ polynomial} \pm 100$ years or $t_{max\ polynomial} \pm 100$ years respectively (see Figure S2 for illustration).

In cases where no change was registered for all of the three climate variables, we assume that the event was not registered at the site. As a measure of the accuracy of the DTW method to identify D-O events, we compared the number of identified events with the number of D-O events that should occur during the time covered by each record (Table 1). To assess whether events were missed in a particular record due to low sampling resolution, we examined the number of samples present in the 900-year interval covering the sampled D-O (i.e. 300 years before to 600 years after the official start date of each event), where low resolution was defined as ≤ 3 samples in this 900-year interval. Reconstructions covering intervals where a signal was not identified were not used in subsequent analyses.

We calculated sample-specific errors for the minimum and maximum reconstructed values. Assuming that the minimum and maximum values are independent, we used error propagation to obtain the error of the change:

$$\sigma_{change} = \sqrt{\sigma_{min}^2 + \sigma_{max}^2}$$

Following Liu et al. (2022), we used a maximum likelihood method to estimate the ratio of ΔMTCO to ΔMTWA (and ratio of Δα to ΔMTWA) to take account of the errors on both variables.

3. Results

*fx*TWA-PLS reproduces the modern climate reasonably well (Table 2; Figure S3). The performance is best for MTCO ($R^2 = 0.75$, RMSEP = 6.51, slope = 0.85) but is also good for MTWA ($R^2 = 0.59$, RMSEP = 3.68, slope = 0.71) and α ($R^2 = 0.65$, RMSEP = 0.18, slope = 0.71). Assessment of the variance inflation factor scores shows that there is no problem of multicollinearity so that it is possible to reconstruct all three climate variables independently (Liu et al., 2023).

The use of dynamic time warping made it possible to identify D-O events robustly (Figure S4.1 ~ S4.8; Table 1; Supplementary Table 1). Thirteen of the 73 sites cover some part of the 50-30 ka periods but do not include D-O events. Across the remaining 60 sites, we identified 298 out

of the 348 individual D-O events (86 %) that should occur during the intervals covered by the records. In the majority of cases where a D-O event should have been registered but could not be identified in an individual record (44 out of 50 cases), the resolution of that part of the record was extremely poor (≤ 3 samples in the 900-year interval starting 300 years before to 600 years after the official start date of the event).

Changes in both MTCO and MTWA were generally largest in the extratropics and were more muted in the tropics (Figure 3). The change in MTCO was significantly larger in the northern extratropics when considered across all D-O events and sites; the change in MTCO was larger, but not significantly larger, in the southern extratropics and the tropics (Table 3). There is a significant positive relationship between the change in α and the change in MTWA in all regions (Figure 4; Table 4).

The spatial patterns of changes in MTCO and MTWA show consistent features across multiple D-O events (Figure 5), most noticeably that the largest warming occurs in the extratropics of Eurasia, while western North America and the southern extratropics are characterised by cooling. The anti-phasing between the northern and southern extratropics is consistent across D-O events. Nevertheless, both the magnitude of the changes and the spatial patterns vary between the D-O events (Figure S5.1; Figure S5.2). Changes in α broadly follow the changes in temperature, with increased α in regions characterised by warming (Figure 5) but show more variability both spatially and between D-O events (Figure S5.3). This is particularly true for Europe, which is characterised by a mixed signal of drying and wetting (Figure S5.3).

4. Discussion and Conclusions

We have presented a first attempt to map the spatial patterns of quantitative changes in seasonal temperature and plant-available moisture during D-O events globally, using a consistent methodology and a single data source. These analyses show that there is an anti-phasing between changes in the northern extratropics and the southern extratropics, with warming in the north and cooling in the south. The largest and most consistent warming during D-O events occurs in Eurasia. There is a significant difference in the warming during winter and summer in the northern extratropics, resulting in an overall reduction in seasonality, but no significant difference in the tropics and southern extratropics. Site-based reconstructions (e.g. Denton et al., 2022; Zander et al., 2024) suggest much larger cooling in winter than summer during cold phases of the last glacial, implying enhanced seasonality compared to warm intervals, which

would be consistent with our reconstructions of a reduction in seasonality during warming events in the northern extratropics. Globally, there is a positive relationship between the change in temperature and plant available moisture, as indicated by α. This is consistent with more qualitative interpretation of palaeo-records from specific regions, where many regions are characterised by both warming and wetting (e.g. western Europe: Sánchez Goñi et al., 2008; Fletcher et al., 2010; eastern Europe: Fleitmann et al., 2009; Stockehecke et al., 2016; central Siberia: Grygar et al., 2006; the Great Basin USA: Denniston et al., 2007; Jiménez-Moreno et al., 2010). However, according to our reconstructions, the nature of this relationship varies between regions: there are some regions that are characterised by warming and wetting, others are characterised by warming and drying (Figure 4, Figure 5). Previous studies have also indicated drier conditions during D-O events, particularly in parts of the USA such as the Pacific Northwest (Grigg and Whitlock, 2002) and Florida (Grimm et al., 2006; Jiménez-Moreno et al., 2010). Although there is some consistency in the broadscale patterns of changes across D-O events, the magnitude of the changes as well as the spatial patterning varies between events (Figure S5.1~ 5.3).

These reconstructions can be used as targets for model evaluation, specifically the two transient D-O experiments planned for the next phase of the Palaeoclimate Modelling Intercomparison (see Malmierca-Vallet et al., 2023 for the experimental protocol). The first of these experiments is a baseline simulation starting at 34 ka, a time with low obliquity, moderate MIS3 greenhouse gas values, and an intermediate ice sheet configuration, which appears to be most conducive to generating D–O-like behaviour in climate models. The second experiment involves the addition of freshwater, to examine whether this is necessary to precondition a state conducive to generating D–O events. The observed anti-phasing in temperature changes between the northern and southern hemispheres is a general feature of climate model experiments. Most models show larger warming in winter than in summer in the northern hemisphere (e.g. Flückiger et al., 2008; Van Meerbeeck et al., 2011; Izumi et al., 2023), which is also consistent with our reconstructions. Models generally show an intensification of the northern hemisphere monsoons during D-O events (e.g. Menviel et al., 2020; Izumi et al, 2023), but there is less consistency about changes in plant-available moisture in the extratropics. Our reconstructions of α suggest an intensification of the northern hemisphere monsoons, consistent with the simulations, and provide an opportunity to evaluate spatial patterns of moisture changes over the extratropics. The reconstructions also indicate an increase in α across much of the tropics, including northern South America, West Africa and southern China and Japan (Figure 5).

Although α is not a direct reflection of summer precipitation, these changes are consistent with enhanced northern hemisphere monsoons during warming events, as shown by speleothem records from the Caribbean (Warken et al, 2019) and speleothem and pollen records from Asia (Wang et al., 2001; Zorzi et al., 2022; Fohlmeister et al., 2023).

Identifying D-O events in pollen records is often problematic, particularly in regions where warming (especially if accompanied by dryer conditions) leads to a reduction (or an hiatus) in sedimentation as reflected in the variable resolution of the available pollen records (e.g. Sinopoli et al., 2019; Wei et al., 2021; Camuera et al., 2022; Pini et al., 2022). The use of shorter periods (Alshehri et al., 2019) goes some way to improving the identification of potential D-O events using dynamic time warping (Alshehri et al., 2019). Thus, we were able to identify 86% of the 348 individual D-O events that should occur during the intervals covered by the 60 records available globally. It is also likely that some of the variability in the reconstructed changes between different D-O events reflects imperfect identification of specific events because of the comparatively modest resolution of the records. Several new high-resolution records covering MIS3 have become available since the compilation of the ACER database (e.g. Bird et al., 2024; Wei et al., 2021; Camuera et al., 2022; Pini et al., 2022; Rowe et al., 2024; Shichi et al., 2023; Zorzi et al., 2022) and including these newer records could help to improve the reliability of the global reconstructions presented here.

Data and code availability. All the data used are public access and cited here. The code used to generate the reconstructions and figures is available at https://github.com/ml4418/DO-climate-reconstruction-paper.git

Author contributions. ML, SPH and ICP designed the study. ML made the reconstructions and produced the figures and tables. ML and SPH carried out the analyses. SPH wrote the first draft of the paper and all authors contributed to the final draft.

Competing Interests. The authors declare not competing interests.

Acknowledgements. ML acknowledges support from Imperial College through the Lee Family Scholarship. ICP acknowledges support from the ERC under the European Union Horizon 2020 research and innovation programme (grant agreement no.: 787203 REALM).

SPH acknowledges fruitful discussions with colleagues from the D-O community working group.

References

Adolphi, F., Bronk Ramsey, C., Erhardt, T., Edwards, R. L., Cheng, H., Turney, C. S. M., Cooper, A., Svensson, A., Rasmussen, S. O., Fischer, H., and Muscheler, R.: Connecting the Greenland ice-core and U / Th timescales via cosmogenic radionuclides: testing the synchroneity of Dansgaard–Oeschger events, Clim. Past, 14, 1755–1781, https://doi.org/10.5194/cp-14-1755-2018, 2018.

Alshehri, M., Coenen, F., and Dures, K.: Effective sub-sequence-based dynamic time warping. In: Bramer, M., Petridis, M. (eds) Artificial Intelligence XXXVI. SGAI 2019. Lecture Notes in Computer Science, 11927. Springer, Cham. https://doi.org/10.1007/978-3-030-34885-4_23, 2019.

Ampel, L., Bigler, C., Wohlfarth, B., Risberg, J., Lotter, A.F., and Veres, D.: Modest summer temperature variability during DO cycles in western Europe, Quat. Sci. Rev., 29, 1322–1327, https://doi.org/10.1016/j.quascirev.2010.03.002, 2010.

Bauska, T. K., Marcott, S. A. and Brook, E. J.: Abrupt changes in the global carbon cycle during the last glacial period, Nat. Geosci., 14(2), 91–96, doi:10.1038/s41561-020-00680-2, 2021.

Bellman, R., and Kalaba, R.: On adaptive control processes, Automatic Control, IRE Transactions, 4, 1–9, http://ieeexplore.ieee.org/xpls/abs all.jsp? arnumber=1104847, 1959.

Bird, M., Brand, M., Comley, R., Fu, X., Hadeen, X., Jacobs, Z., Rowe, C., Wurster, C., Zwart, C. and Bradshaw, C.: Late Pleistocene emergence of an anthropogenic fire regime in Australia's tropical savannahs, Nat. Geosci., 17, doi:10.1038/s41561-024-01388-3, 2024.

Burstyn, Y., Gazit, A., and Omri Dvir, O.: Hierarchical Dynamic Time Warping methodology for aggregating multiple geological time series, Comp. & Geosci., 150, 104704, https://doi.org/10.1016/j.cageo.2021.104704, 2021.

Camuera, J., Ramos-Román, M.J., Jiménez-Moreno, G. *et al.*: Past 200 kyr hydroclimate variability in the western Mediterranean and its connection to the African Humid Periods, Sci. Rep., 12, 9050, https://doi.org/10.1038/s41598-022-12047-1, 2022.

Corrick, E.C., Drysdale, R.N., Hellstrom, J.C., Capron, E., Rasmussen, S.O., Zhang, X., Fleitmann, D., Couchoud, I., and Wolff, E.: Synchronous timing of abrupt climate changes during the last glacial period, Science, 369, 963–969, https://doi.org/10.1126/science.aay5538, 2020.

Crisp, M. D. and Cook, L. G.: Phylogenetic niche conservatism: What are the underlying evolutionary and ecological causes?, New Phytol., 196(3), 681–694, doi:10.1111/j.1469-8137.2012.04298.x, 2012.

Dansgaard, W., Johnsen, S.J., Clausen, H.B., Dahl-Jensen, D., Gundestrup, N.S., Hammer, C.U., Hvidberg, C.S., Steffensen, J.P., Sveinbjörnsdottir, A.E., Jouzel, J., and Bond, G.: Evidence for general instability of past climate from a 250-kyr ice-core record, Nature, 364, 218–220, https://doi.org/10.1038/364218a0, 1993.

Denniston, R.F., Asmerom, Y., Polyak, V., Dorale, J.A., Carpenter, S.J., Trodick, C., Hoye, B., and González, L.A.: Synchronous millennial-scale climatic changes in the Great Basin and the North Atlantic during the last interglacial. Geology 35, 619-622, 2007.

Doblas-Reyes, F. J., Sörensson, A. A., Almazroui, M., Dosio, A., Gutowski, W. J., Haarsma, R., Hamdi, R., Hewitson, B., Kwon, W.-T., Lamptey, B. L., Maraun, D., Stephenson, T. S., Takayabu, I., Terray, L., Turner, A. and Zuo, Z.: Linking global to regional climate change, in Climate Change 2021 – The Physical Science Basis: Working Group I Contribution to the Sixth Assessment Report of the Intergovernmental Panel on Climate Change, edited by V. Masson-Delmotte, P.Zhai, A. Pirani, S. L. Connors, C. Péan, S. Berger, N. Caud, Y. Chen, L. Goldfarb, M. I. Gomis, M. Huang, K. Leitzell, E.Lonnoy, J. B. R. Matthews, T. K. Maycock, T. Waterfield, O. Yelekçi, R. Yu, and B. Zhou, pp. 1363–1512, Cambridge University Press, Cambridge, United Kingdom and New York, NY, USA., 2021.Fleitmann, D., Cheng, H., Badertscher, S., Edwards, R.L.,

Mudelsee, M., Göktürk, O.M., Fankhauser, A., Pickering, R., Raible, C.C., Matter, A., Kramers, J., and Tüysüz, O.: Timing and climatic impact of Greenland interstadials recorded in stalagmites from northern Turkey, Geophys. Res. Lett., 36, 2009.

Fletcher, W.F., Sánchez Goñi, M.F., Allen, J.R.M., Cheddadi, R., Combourieu-Nebout, N., Huntley, B., Lawson, I., Londeix, L., Magri, D., Margari, V., Müller, U.C., Naughton, F., Novenko, E., Roucoux, K., Tzedakis, P.C.: Millennial-scale variability during the last glacial in vegetation records from Europe, Quat. Sci. Rev., 29, 2839-2864, https://doi.org/10.1016/j.quascirev.2009.11.015, 2010.

Flückiger, J., Knutti, R., White, J.W.C., and Renssen, H.: Modeled seasonality of glacial abrupt climate events, Clim. Dyn., 31, 633–645, https://doi.org/10.1007/s00382-008-0373-y, 2008.

Fohlmeister, J., Sekhon, N., Columbu, A., Vettoretti, G., Weitzel, N., Rehfeld, K., Veiga-Pires, C., Ben-Yami, M., Marwan, N. and Boers, N.: Global reorganization of atmospheric circulation during Dansgaard–Oeschger cycles, Proc. Natl. Acad. Sci., 120(36), e2302283120, doi:10.1073/pnas.2302283120, 2023.

Grigg, L.D., and Whitlock, C.: Patterns and causes of millennial-scale climate change in the Pacific Northwest during Marine Isotope Stages 2 and 3, Quat. Sci. Rev., 21, 2067-2083, 2002.

Grimm, E.C., Watts, W.A., Jacobson, G.L., Hansen, B.C.S., Almquist, H., and Dieffenbacher-Krall, A.C.: Evidence for warm wet Heinrich events in Florida, Quat. Sci. Rev., 25, 2197-2211, 2006.

Grygar, T., Kadlec, J., Pruner, P., Swann, G., Bezdicka, P., Hradil, D., Lang, K., Novotna, K., and Oberhänsli, H.: Paleoenvironmental record in Lake Baikal sediments: environmental changes in the last 160 ky, Palaeogeogr. Palaeoclimatol. Palaeoecol., 237, 240-254, 2006.

Guiot, J., de Beaulieu, J. L., Cheddadi, R., David, F., Ponel, P., and Reille, M.: The climate in Western Europe during the last Glacial/Interglacial cycle derived from pollen and insect remains, Palaeogeogr., Palaeoclimatol., Palaeoecol., 103, 73–93, https://doi.org/10.1016/0031-0182(93)90053-L, 1993.

Jiménez-Moreno, G., Anderson, R.S., Desprat, S., Grigg, L.D., Grimm, E.C., Heusser, L.E., Jacobs, B.F., López-Martínez, C., Whitlock, C.L., and Willard, D.A.:Millennial-scale variability during the last glacial in vegetation records from North America, Quat. Sci. Rev., 29, 2865-2881, https://doi.org/10.1016/j.quascirev.2009.12.013, 2010.

Harrison, S.P., and Sánchez Goñi, M.F.: Global patterns of vegetation response to millennial-scale variability during the last glacial: A synthesis. Quat. Sci. Rev., 29, 2957-2980, 2010.

Harvey, P. H. and Pagel, M. D.: The comparative method in evolutionary biology, Oxford University Press., 1991.

Huber, C., Leuenberger, M., Spahni, R., Flückiger, J., Schwander, J., Stocker, T.F., Johnsen, S., Landais, A., and Jouzel, J.: Isotope calibrated Greenland temperature record over Marine Iso- tope Stage 3 and its relation to CH_4, Earth Planet. Sci. Lett., 243, 504–519, 2006.

Huntley, B., Bartlein, P. J. and Prentice, I. C.: Climatic control of the distribution and abundance of Beech (Fagus L.) in Europe and North America, J. Biogeogr., 16(6), 551–560, doi:10.2307/2845210, 1989.

Huntley, B., Watts, W.A., Allen, J.R.M., Zolitschka, B.: Palaeoclimate, chronology and vegetation history of the Weichselian Lateglacial: comparative analysis of data from three cores at Lago Grande di Monticchio, southern Italy, Quat. Sci. Rev.,18: 945-960, https://doi.org/10.1016/S0277-3791(99)00007-4, 1999.

IPCC: Climate change 2022: Impacts, adaptation and vulnerability. Contribution of working group II to the sixth assessment report of the Intergovernmental Panel on Climate Change, edited by H.-O. Pörtner, D. C. Roberts, M. Tignor, E. S. Poloczanska, K. Mintenbeck, A. Alegría, M. Craig, S. Langsdorf, S. Löschke, V. Möller, A. Okem, and B. Rama, Cambridge University Press, Cambridge University Press, Cambridge, UK and New York, NY, USA., 2022.

Jiang, K., Wang, Q., Dimitrov, D., Luo, A., Xu, X., Su, X., Liu, Y., Li, Y., Li, Y. and Wang, Z.: Evolutionary history and global angiosperm species richness–climate relationships, Glob. Ecol. Biogeogr., 32(7), 1059–1072, doi:10.1111/geb.13687, 2023.

Kindler, P., Guillevic, M., Baumgartner, M., Schwander, J., Landais, A., and Leuenberger, M.: Temperature reconstruction from 10 to 120 kyr b2k from the NGRIP ice core, Clim. Past, 10, 887–902, https://doi.org/10.5194/cp-10-887-2014, 2014.

Lee, J.-Y., Marotzke, J., Bala, G., Cao, L., Corti, S., Dunne, J. P., Engelbrecht, F., Fischer, E., Fyfe, J. C., Jones, C., Maycock, A., Mutemi, J., Ndiaye, O., Panickal, S. and Zhou, T.: Future global climate: Scenario-based projections and near- term information, in Climate change 2021: The physical science basis. Contribution of working group I to the sixth assessment report of the Intergovernmental Panel on Climate Change, edited by V. Masson-Delmotte, P. Zhai, A. Pirani, S. L. Connors, C. Péan, S. Berger, N. Caud, Y. Chen, L. Goldfarb, M. I. Gomis, M. Huang, K. Leitzell, E. Lonnoy, J. B. R. Matthews, T. K. Maycock, T. Waterfield, O. Yelekçi, R. Yu, and B. Zhou, pp. 553–672, Cambridge University Press, Cambridge, United Kingdom and New York, NY, USA., 2021.

Liu, M., Prentice, I.C., ter Braak, C.J.F, and Harrison, S.P.: An improved statistical approach for reconstructing past climates from biotic assemblages, Proc. Royal Soc., Math. A, 476, 20200346, 20200346, https://doi.org/10.1098/rspa.2020.0346, 2020.

Liu, M., Shen, Y., González-Sampériz, P., Gil-Romera, G., ter Braak, C.J.F. Prentice, I.C., and Harrison, S.P.: Holocene climates of the Iberian Peninsula, Clim. Past 19, 803-834, https://doi.org/10.5194/cp-19-803-2023, 2023.

Malmierca-Vallet, I., Sime, L.C., and the D–O community members: Dansgaard–Oeschger events in climate models: review and baseline Marine Isotope Stage 3 (MIS3) protocol, Clim. Past, 19, 915–942, https://doi.org/10.5194/cp-19-915-2023, 2023.

Menviel, L., Timmermann, A., Friedrich, T., and England, M. H.: Hindcasting the continuum of Dansgaard–Oeschger variability: mechanisms, patterns and timing, Clim. Past 10, 63–77, 2014.

Menviel, L.C., Skinner, L.C., Tarasov, L., and Tzedakis, P.C.: An ice–climate oscillatory framework for Dansgaard–Oeschger cycles, Nat. Rev. Earth Environ., 1, 677–693, https://doi.org/10.1038/s43017-020-00106-y, 2020.

449 Peterson, A. T.: Ecological niche conservatism: A time-structured review of evidence, J.
450 Biogeogr., 38(5), 817–827, doi:10.1111/j.1365-2699.2010.02456.x, 2011.

451 Pini, R., Furlanetto, G., Vallé, F., Badino, F., Wick, L., Anselmetti, F.S., Bertuletti, P., Fusi, N.,
452 Morlock, M.A., Delmonte, B., Harrison, S.P., Maggi, V., Ravazzi, C.: Linking North
453 Atlantic and Alpine Last Glacial Maximum climates via a high-resolution pollen-based
454 subarctic forest steppe record, Quat. Sci. Rev., 294, 107759,
455 https://doi.org/10.1016/j.quascirev.2022.107759, 2022.

456 Prentice, I. C., Cleator, S. F., Huang, Y. H., Harrison, S. P. and Roulstone, I.: Reconstructing
457 ice-age palaeoclimates: Quantifying low-CO_2 effects on plants, Glob. Planet. Change,
458 149, 166–176, doi:https://doi.org/10.1016/j.gloplacha.2016.12.012, 2017.

459 Prentice, I. C., Villegas-Diaz, R. and Harrison, S. P.: Accounting for atmospheric carbon
460 dioxide variations in pollen-based reconstruction of past hydroclimates, Glob. Planet.
461 Change, 211, 103790, doi:10.1016/j.gloplacha.2022.103790, 2022.

462 Prud'homme, C., Fischer, P., Jöris, O., Gromov, S., Vinnepand, M., Hatté, C., Vonhof, H.,
463 Moine, O., Vött, A., and Fitzsimmons, K. E.: Millennial-timescale quantitative
464 estimates of climate dynamics in central Europe from earthworm calcite granules in
465 loess deposits, Commun. Earth Environ., 3, 1–14, https://doi.org/10.1038/s43247-022-
466 00595-3, 2022.

467 Rowe, C., Brand, M., Wurster, C. M. and Bird, M. I.: Vegetation changes through stadial and
468 interstadial stages of MIS 4 and MIS 3 based on a palynological analysis of the
469 Girraween Lagoon sediments of Darwin, Australia, Palaeogeogr. Palaeoclimatol.
470 Palaeoecol., 642, 112150, doi:10.1016/j.palaeo.2024.112150, 2024.

471 Sánchez Goñi, M., Cacho, I., Turon, J., Guiot, J., Sierro, F., Peypouquet, J., Grimalt, J. and
472 Shackleton, N.: Synchroneity between marine and terrestrial responses to millennial
473 scale climatic variability during the last glacial period in the Mediterranean region,
474 Clim. Dyn., 19(1), 95–105, doi:10.1007/s00382-001-0212-x, 2002.

475 Sánchez Goñi, M.F., and Harrison, S.P.: Millennial-scale climate variability and vegetation
476 changes during the Last Glacial: Concepts and terminology, Quat. Sci. Rev., 29, 2823–
477 2827, 2010.

478 Sánchez Goñi, M.F., Desprat, S., Daniau, A.-L., Bassinot, F., Polanco-Martínez, J.M., Harrison,
479 S.P., Allen, J.R.P., Anderson, R.S., Behling, H., Bonnefille, R., Burjachs, F., Carrión,
480 J.S., Cheddadi, R., Clark, J.S., Combourieu-Nebout, N., Courtney-Mustaphi, C.,
481 Debusk, G.H., Dupont, L.M., Finch, J., Fletcher, W.J., Giardini, M., González, C.,
482 Gosling, W.D., Grigg, L.D., Grimm, E.C., Hayashi, R., Helmens, K., Heusser, L.E.,
483 Hill, T., Hope, G., Huntley, B., Igarashi, Y., Irino, T., Jacobs, B.F., Jiménez-Moreno, G.,
484 Kawai, S., Kershaw, P., Kumon, F., Lawson, I., Ledru, M.-P., Lézine, A.-M., Liew, P.-
485 M., Magri, D., Marchant, R., Margari, V., Mayle, F., McKenzie, M., Moss, P., Müller,
486 S., Müller, U.C., Naughton, F., Newnham, R.M., Oba, T., Pérez-Obiol, R., Pini, R.,
487 Ravazzi, C., Roucoux, K.H., Rucina, S., Scott, L., Takahara, H., Tzedakis, P.C., Urrego,
488 D.H., Van Geel, B., Valencia, B.G., Vandergoes, M.J., Vincens , A., Whitlock, C.L.,
489 Willard, D. A., and Yamamoto, M.: The ACER pollen and charcoal database: a global
490 resource to document vegetation and fire response to abrupt climate changes of the last
491 glacial period, Earth Syst. Sci. Data 9: 679-695, 2017.

492 Shichi, K., Goebel, T., Izuho, M. and Kashiwaya, K.: Climate amelioration, abrupt vegetation
493 recovery, and the dispersal of Homo sapiens in Baikal Siberia, Sci. Adv., 9(38),
494 eadi0189, doi:10.1126/sciadv.adi0189, 2024.

495 Sinopoli, G., Peyron, O., Masi, A., Holtvoeth, J., Francke, A., Wagner, B., and Sadori, L.:
496 Pollen-based temperature and precipitation changes in the Ohrid Basin (western
497 Balkans) between 160 and 70 ka, Clim. Past, 15, 53–71, https://doi.org/10.5194/cp-15-
498 53-2019, 2019.

499 Stockhecke, M., Timmermann, A., Kipfer, R., Haug, G.H., Kwiecien, O., Friedrich, T.,
500 Menviel, L., Litt, T., Pickarski, N., and Anselmetti, F.S.: Millennial to orbital-scale
501 variations of drought intensity in the Eastern Mediterranean, Quat. Sci. Rev., 133, 77-
502 95, 2016.

503 Turner, M. G., Wei, D., Prentice, I. C. and Harrison, S. P.: The impact of methodological
504 decisions on climate reconstructions using WA-PLS, Quat. Res., 99, 341–356,
505 doi:10.1017/qua.2020.44, 2021.

506 Újvári, G., Bernasconi, S. M., Stevens, T., Kele, S., Páll-Gergely, B., Surányi, G., and Demény,
507 A.: Stadial-Interstadial Temperature and Aridity Variations in East Central Europe

508 Preceding the Last Glacial Maximum, Paleoceanog. Paleoclim., 36, e2020PA004170,
509 https://doi.org/10.1029/2020PA004170, 2021.

510 Van Meerbeeck, C.J., Renssen, H., Roche, D.M., Wohlfarth, B., Bohncke, S.J.P., Bos, J.A.A.,
511 Engels, S., Helmens, K.F., Sánchez-Goñi, M.F., Svensson, A., and Vandenberghe, J.:
512 The nature of MIS 3 stadial-interstadial transitions in Europe: New insights from
513 model-data comparisons, Quat. Sci. Rev., 30, 3618–3637,
514 https://doi.org/10.1016/j.quascirev.2011.08.002, 2011.

515 Villegas-Diaz, R., and Harrison, S.P.: The SPECIAL Modern Pollen Data Set for Climate
516 Reconstructions, version 2 (SMPDSv2). University of Reading.
517 Dataset. https://doi.org/10.17864/1947.000389, 2022.

518 Voelker, A.H.: Global distribution of centennial-scale records for Marine Isotope Stage (MIS)
519 3: a database, Quat. Sci. Rev., 21, 1185–1212, 2002.

520 Wang, Y. J., Cheng, H., Edwards, R. L., An, Z. S., Wu, J. Y., Shen, C.-C. and Dorale, J. A.: A
521 high-resolution absolute-dated Late Pleistocene monsoon record from Hulu Cave,
522 China, Science (80-.)., 294(5550), 2345–2348, doi:10.1126/science.1064618, 2001.

523 Warken, S. F., Scholz, D., Spötl, C., Jochum, K. P., Pajón, J. M., Bahr, A. and Mangini, A.:
524 Caribbean hydroclimate and vegetation history across the last glacial period, Quat. Sci.
525 Rev., 218, 75–90, doi:10.1016/j.quascirev.2019.06.019, 2019.

526 Wei, D., González-Sampériz, P., Gil-Romera, G., Harrison, S.P., and Prentice, I.C.: Seasonal
527 temperature and moisture changes in interior semi-arid Spain from the last interglacial
528 to the Late Holocene, Quat. Res., 101, 143–155, https://doi.org/10.1017/qua.2020.108,
529 2021.

530 Wiens, J. and Graham, C.: Niche conservatism: Integrating evolution, ecology, and
531 conservation biology, Annu. Rev. Ecol. Evol. Syst., 36, 519–539,
532 doi:10.1146/annurev.ecolsys.36.102803.095431, 2005.

533 Wolff, E. W., Chappellaz, J., Blunier, T., Rasmussen, S. O. and Svensson, A.: Millennial-scale
534 variability during the last glacial: The ice core record, Quat. Sci. Rev., 29(21), 2828–
535 2838, doi:10.1016/j.quascirev.2009.10.013, 2010.

536 Yin, X., Jarvie, S., Guo, W.-Y., Deng, T., Mao, L., Zhang, M., Chu, C., Qian, H., Svenning, J.-
537 C. and He, F.: Niche overlap and divergence times support niche conservatism in
538 eastern Asia–eastern North America disjunct plants, Glob. Ecol. Biogeogr., 30(10),
539 1990–2003, doi:10.1111/geb.13360, 2021.

540 Zander, P. D., Böhl, D., Sirocko, F., Auderset, A., Haug, G. H. and Martínez-García, A.:
541 Reconstruction of warm-season temperatures in central Europe during the past 60 000
542 years from lacustrine branched glycerol dialkyl glycerol tetraethers (brGDGTs), Clim.
543 Past, 20(4), 841–864, doi:10.5194/cp-20-841-2024, 2024.

544 Zorzi, C., Desprat, S., Clément, C., Thirumalai, K., Oliviera, D., Anupama, K., Prasad, S. and
545 Martinez, P.: When eastern India oscillated between desert versus savannah-dominated
546 vegetation, Geophys. Res. Lett., 49(16), e2022GL099417,
547 doi:10.1029/2022GL099417, 2022.

548

549 **Figures and Tables**

550 Figure 1: Map showing the locations of sites (a) from the Abrupt Climate Changes and
551 Environmental Responses (ACER) database (Sánchez Goñi et al., 2017) covering the interval
552 between 50 ka and 30 ka used for the reconstructions and (b) sites in version 2 of the SPECIAL
553 Modern Pollen Data Set (SMPDSv2: Villegas-Diaz and Harrison, 2022) used to derive the
554 transfer functions for these climate reconstructions.

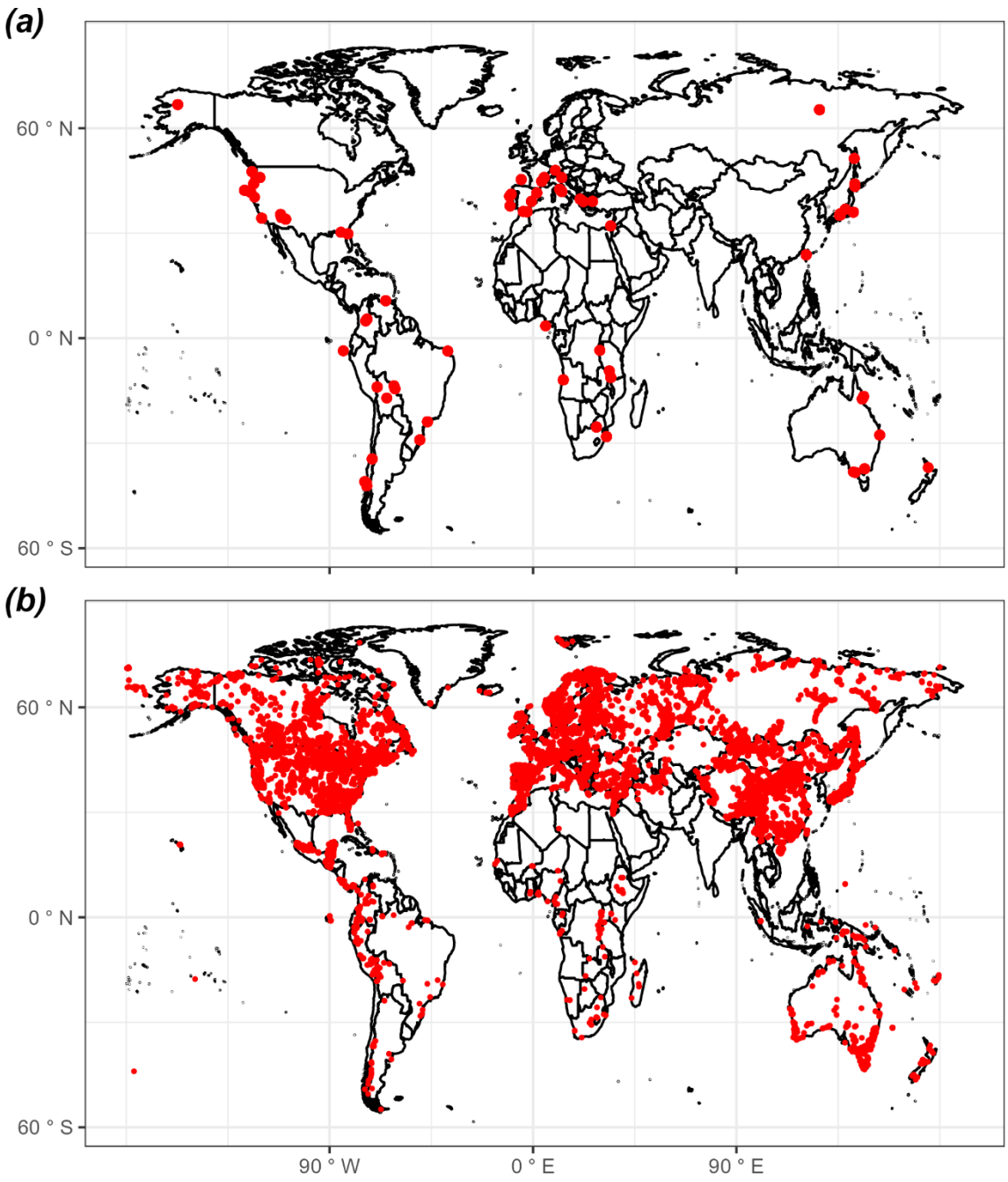

555

556

Figure 2: Flow chart showing the reconstruction methodology.

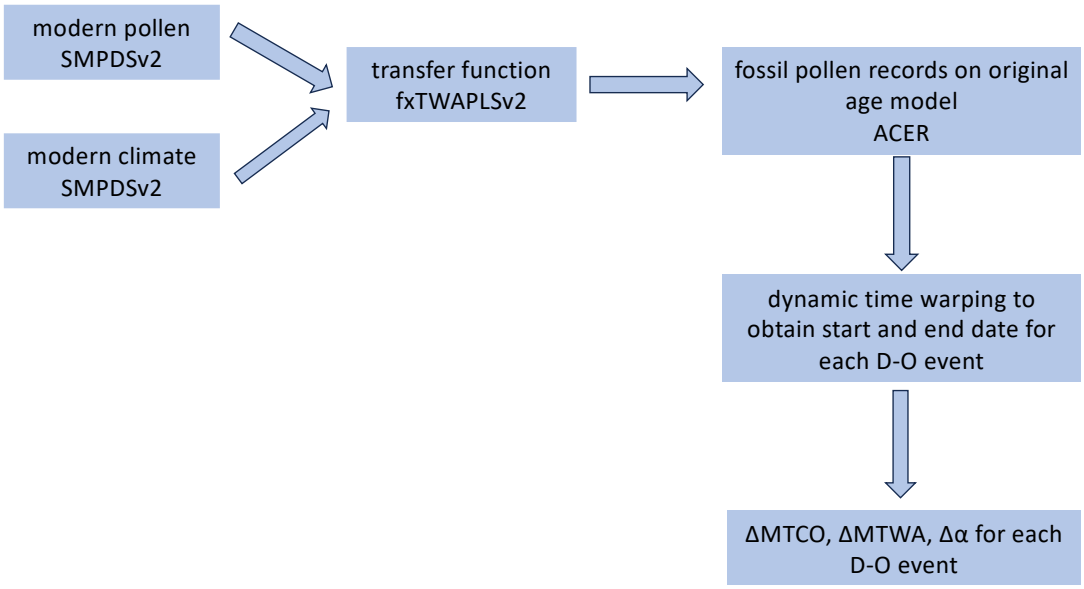

Figure 3: Scatter plot of the change in mean temperature of the coldest month (ΔMTCO) versus the change in mean temperature of the warmest month (ΔMTWA) during individual Dansgaard-Oeschger (D-O) events at individual sites. The points are colour-coded to indicate whether the sites are from the northern extratropics (NET, north of 23.5°N), the tropics (TROP, between 23.5°N and 23.5°S) or southern extratropics (SET, south of 23.5°S).

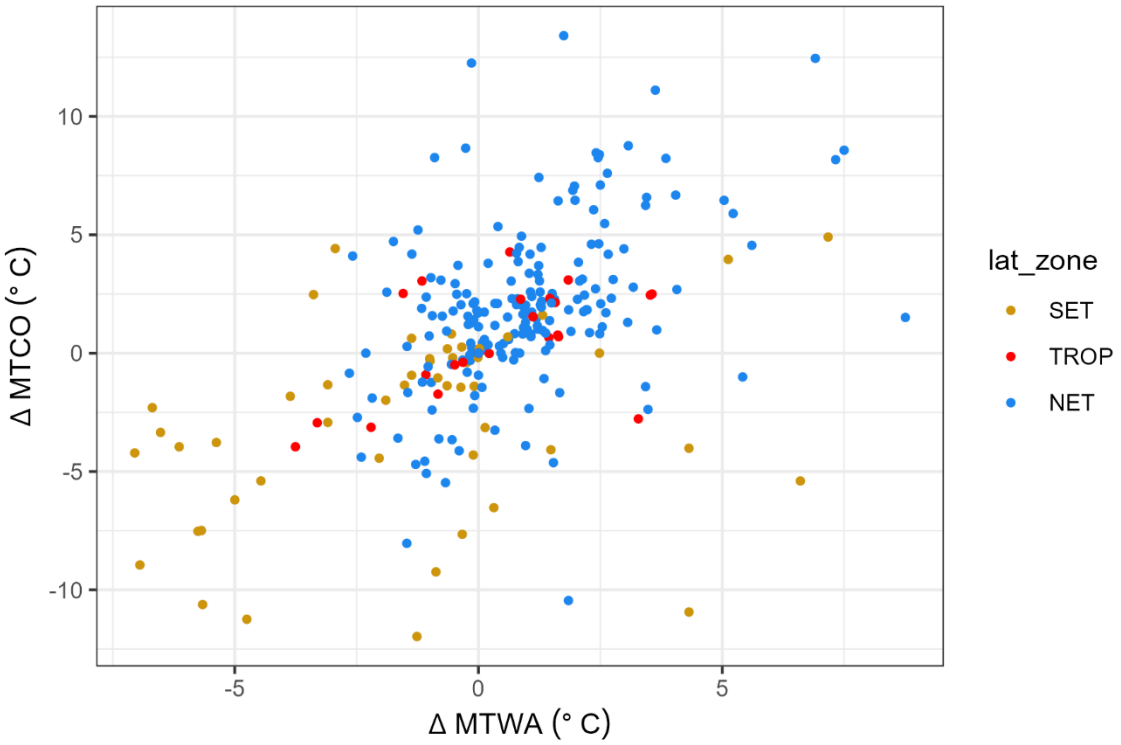

Figure 4: Scatter plot of the change in plant-available moisture (Δα) versus the change in mean temperature of the warmest month (ΔMTWA) during individual Dansgaard-Oeschger (D-O) events at individual sites. The points are colour-coded to indicate whether the sites are from the northern extratropics (NET, north of 23.5°N), the tropics (TROP, between 23.5°N and 23.5°S) or southern extratropics (SET, south of 23.5°S).

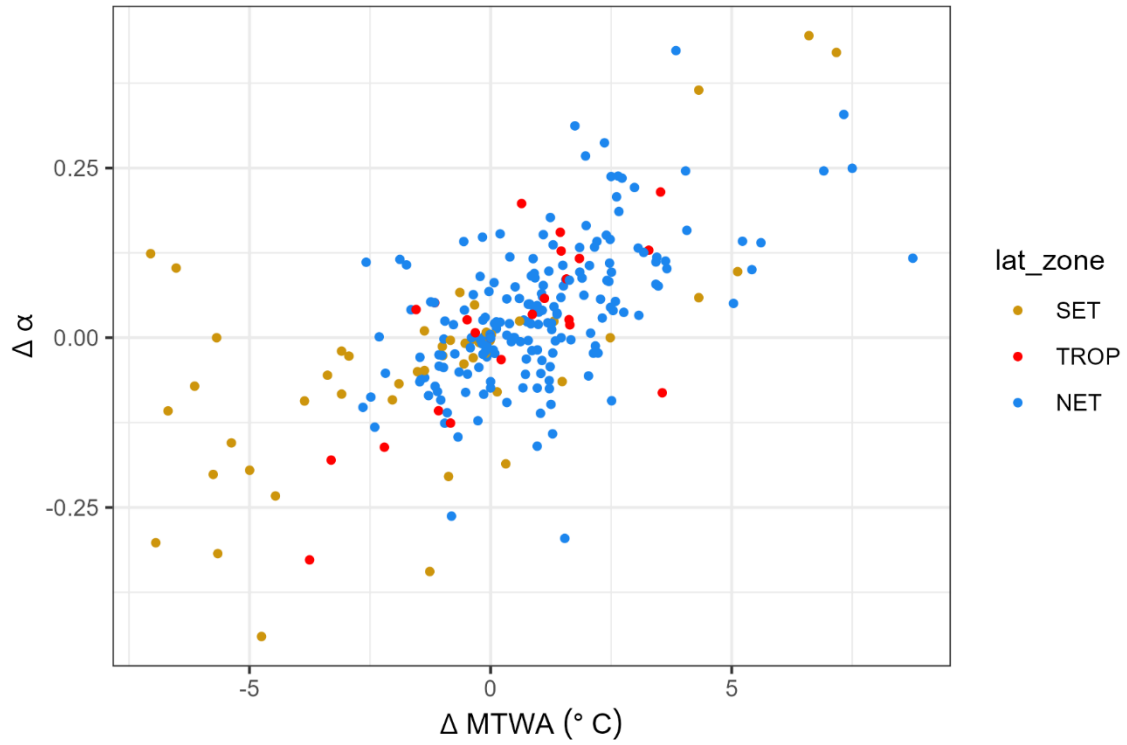

576 Figure 5: Maps showing the median change of site-based reconstructions for Dansgaard-
577 Oeschger (D-O) events.

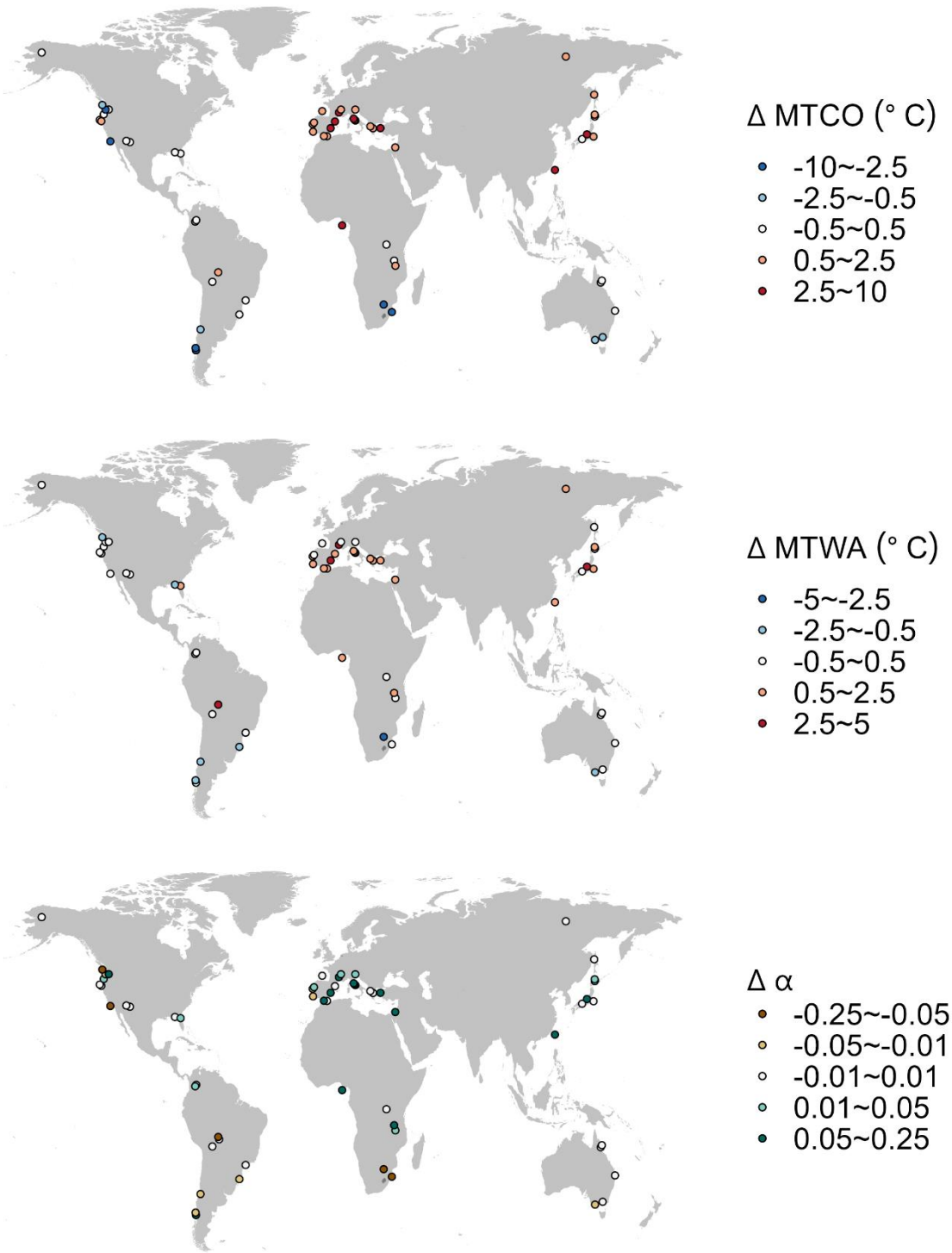

578

579

Table 1: Details of the sites from the Abrupt Climate Changes and Environmental Responses (ACER) database (Sánchez Goñi et al., 2017) covering the interval between 50 ka and 30 ka used for the climate reconstructions. n_{due} is the number of D-O events that should be found based on the time interval covered by the record. n_{miss} is the number of D-O events that were not identified. n_{low} is the number of D-O events missed because of low resolution of part of the record. Some of the 73 sites (indicated by NA in n_{due}, n_{miss} and n_{low}) provide records for parts of the 50-30ka interval but not for the intervals of the D-O events. Reconstructions based on samples where the D-O signal was not identified were not used in subsequent analyses. The full citations for each site are given in Supplementary Information.

Site name	Latitude	Longitude	Elevation (m)	Site type	Reference(s)	n_{due}	n_{miss}	n_{low}
Abric Romanì	41.53	1.68	350	TERR	Burjachs & Julià (1994)	2	0	0
Azzano Decimo	45.8833	12.7165	10	TERR	Pini et al. (2009)	6	2	2
Caledonia Fen	–37.3333	146.7333	1280	TERR	Kershaw et al. (2007b)	8	1	1
Cambara do Sul	–29.05	–50.1	1040	TERR	Behling et al. (2004)	7	1	0
Camel Lake	30.26	–85.01	20	TERR	Watts et al. (1992)	2	0	0
Carp Lake	45.91	–120.88	720	TERR	Whitlock and Bartlein (1997); Whitlock et al. (2000)	8	1	1
Colônia	-23.87	-46.71	900	TERR	Ledru et al. (2009)	7	4	4
Core Trident 163 31B	–3.61	–83.96	–3210	MARI	Heusser and Shackleton (1994)	NA	NA	NA
Fargher Lake	45.88	–122.58	200	TERR	Grigg and Whitlock (2002)	8	1	0
Fundo Nueva	–41.28	–73.83	66	TERR	Heusser et al. (2000)	6	1	0
Fuquene	5.45	–73.46	2540	TERR	van Geel and van der Hammen (1973); Mommersteeg (1998)	7	3	3
Füramoos	47.98	9.88	662	TERR	Müller et al. (2003)	NA	NA	NA
GeoB3104	–3.67	–37.72	–767	MARI	Behling et al. (2000)	NA	NA	NA
Hay Lake	34	–109.425	2780	TERR	Jacobs (1985)	5	3	3
Ioannina	39.75	20.85	470	TERR	Tzedakis et al. (2002); Tzedakis et al. (2004)	8	0	0
Joe Lake	66.76667	–157.217	183	TERR	Anderson (1988); Anderson et al. (1994)	7	3	3
Kalaloch	47.6053	–124.371	19	TERR	Heusser (1972)	8	1	0
Kamiyoshi Basin (KY01)	35.102	135.586	335	TERR	Takahara et al. (2000);; Takahara et al. (2007); Hayashi et al. (2009)	1	0	0
Kashiru Bog	–3.47	29.57	2240	TERR	Bonnefille & Riollet (1988); Bonnefille et al. (1992)	2	1	1
Kenbuchi Basin	44.05	142.383	135	TERR	Igarashi et al. (1993); Igarashi (1996)	3	0	0
Khoe	51.341	142.14	15	TERR	Igarashi et al. (2002)	6	2	2
Kohuora	–36.95	174.8667	5	TERR	Newnham et al. (2007)	NA	NA	NA
Kurota Lowland	35.517	135.879	20	TERR	Takahara & Kitagawa (2000)	NA	NA	NA
KW31	3.52	5.57	–1181	MARI	Lézine & Cazet (2005);	2	0	0

					Lézine et al. (2005)			
La Laguna	4.92	–74.03	2900	TERR	Helmens et al., 1(996)	2	0	0
Lac du Bouchet	44.83	3.82	1200	TERR	Reille and de Beaulieu (1990)	8	0	0
Lagaccione	42.57	11.8	355	TERR	Magri (1999); Magri (2008)	7	0	0
Laguna Bella Vista	–13.6167	–61.55	600	TERR	Burbridge et al. (2004)	2	0	0
Laguna Chaplin	–14.4667	–61.0667	600	TERR	Burbridge et al. (2004)	1	0	0
Lake Billyakh	65.2833	126.7833	340	TERR	Müller et al. (2010)	4	0	0
Lake Biwa (BIW95-4)	35.245	136.054	84	TERR	Takemura et al. (2000); Hayashida et al. (2007); Hayashi et al. (2010)	NA	NA	NA
Lake Consuelo (CON1)	–13.95	–68.991	1360	TERR	Urrego et al. (2005); Urrego et al. (2010)	1	0	0
Lake Malawi	–11.22	34.42	470	TERR	DeBusk (1998)	6	2	2
Lake Masoko	–9.33	33.75	840	TERR	Vincens et al. (2007)	2	0	0
Lake Nojiri	36.831	138.216	657	TERR	Kumon et al. (2009)	8	0	0
Lake Tulane	29.83	–81.95	36	TERR	Grimm et al. (1993); Grimm et al. (2006)	8	2	2
Lake Wangoom LW87 core	–38.35	142.6	100	TERR	Harle et al. (2002)	7	2	2
Lake Xinias	39.05	22.27	500	TERR	Bottema (1979)	8	1	1
Les Echets G	45.9	4.93	267	TERR	de Beaulieu & Reille (1984)	8	0	0
Little Lake	44.16	–123.58	217	TERR	Grigg et al. (2001)	5	0	0
Lynchs Crater	–17.3667	145.7	760	TERR	Kershaw et al. (2007a)	8	1	1
MD01-2421	36.02	141.77	–2224	MARI	Igarashi & Oba (2006); Oba et al. (2006); Aoki et al. (2008)	7	1	0
MD03-2622 Cariaco Basin	10.7061	–65.1691	–877	MARI	González et al. (2008); González and Dupont (2009)	NA	NA	NA
MD04-2845	45.35	–5.22	–4100	MARI	Sánchez Goñi et al. (2008); Daniau et al. (2009)	8	0	0
MD84-629	32.07	34.35	–745	MARI	Cheddadi & Rossignol-Strick (1995)	8	1	1
MD95-2039	40.58	–10.35	–3381	MARI	Roucoux et al. (2001); Roucoux et al. (2005)	8	0	0
MD95-2042	37.8	–10.17	–3148	MARI	Sánchez Goñi et al. (1999); Sánchez Goñi et al. (2000); Daniau et al. (2007); Sánchez Goñi et al. (2008); (Sánchez Goñi et al. (2009)	8	0	0
MD95-2043	36.14	–2.621	–1841	MARI	Sánchez Goñi et al. (2002); Fletcher and Sánchez Goñi (2008)	8	1	1
MD99-2331	41.15	–9.68	–2110	MARI	Sánchez Goñi et al. (2005); Naughton et al. (2007); Sánchez Goñi et al. (2008); Naughton et al. (2009)	8	1	1
Megali Limni	39.1025	26.3208	323	TERR	Margari et al. (2007); Margari et al. (2009)	6	0	0
Mfabeni Peatland	–28.1487	32.51867	11	TERR	Finch & Hill (2008)	5	0	0

Nakafurano	43.367	142.433	173	TERR	Igarashi et al. (1993)	2	0	0
Native Companion Lagoon	–27.68	153.41	20	TERR	Petherick et al. (2008a); Petherick et al. (2008b)	6	0	0
Navarrés	39.1	-0.68	225	TERR	Carrión & van Geel (1999)	3	0	0
ODP 1233 C	–41	–74.45	–838	MARI	Lamy et al. (2004); Heusser et al. (2006)	NA	NA	NA
ODP 820	–16.63	146.3	–280	MARI	Moss & Kershaw (2000); Moss & Kershaw (2007)	7	4	4
ODP site 976	36.2	–4.3	–1108	MARI	Nebout et al. (2002); Masson-Delmotte et al. (2005)	8	1	0
ODP1019	41.66	–124.91	989	MARI	Mix et al. (1999); Pisias et al. (2001)	8	1	1
ODP1078C	–11.92	13.4	–426	MARI	Dupont & Behling (2006); Dupont et al. (2008)	NA	NA	NA
ODP893A	34.28	–120.03	–577	MARI	Heusser (1998); Heusser (2000)	8	1	1
Potato Lake	34.45	–111.33	2222	TERR	Anderson (1993)	4	2	2
Rice Lake (Rice Lake 81)	40.3	–123.22	1100	TERR	L. Heusser, unpublished data	NA	NA	NA
Siberia	–17.09	–64.72	2920	TERR	Mourguiart & Ledru (2003)	1	1	1
Stracciacappa	42.13	12.32	220	TERR	Giardini (2007)	5	1	1
Tagua Tagua	–34.5	–71.16	200	TERR	Heusser (1990)	6	1	1
Taiquemo	–42.17	–73.6	170	TERR	Heusser et al. (1999); Heusser and Heusser (2006)	8	0	0
Toushe Basin	23.82	120.88	650	TERR	Liew et al. (2006)	8	0	0
Tswaing Crater	–25.4	28.08	1100	TERR	Partridge et al. (1997); Scott et al. (2008); L. Scott, unpublished data;	6	0	0
Tyrrendara Swamp	–38.1986	141.7626	13	TERR	Builth et al. (2008)	NA	NA	NA
Valle di Castiglione	41.9	12.76	44	TERR	Alessio et al. (1986); Follieri et al. (1988); Follieri et al. (1989); Narcisi et al. (1992): Narcisi (1999); Magri & Tzedakis (2000); Magri (2008)	7	1	1
W8709-13 PC	42.11	–125.75	–2712	MARI	Pisias et al. (2001)	7	1	1
W8709-8 PC	42.26	–127.68	–3111	MARI	Heusser (1998); Lyle et al. (1992)	NA	NA	NA
Walker Lake	35.38	–111.71	2500	TERR	Berry et al. (1982); Adam et al. (1985); Hevly (1985)	NA	NA	NA

589

590

Table 2. Leave-out cross-validation (with geographically and climatically close sites removed) using fxTWA-PLSv2 for mean temperature of the coldest month (MTCO), mean temperature of the warmest month (MTWA) and plant-available water (α) with P-splines smoothed *fx* estimation and bins of 0.02, 0.02 and 0.002, respectively. *n* is the number of components where the last significant number of components is indicated in **bold**. Avg.bias is the average bias; RMSEP is the root-mean-square error of prediction; and ΔRMSEP is the per cent change of RMSEP, which is $100 \times (\mathrm{RMSEP}_n - \mathrm{RMSEP}_{n-1})/\mathrm{RMSEP}_{n-1}$; when $n = 1$, RMSEP_0 is the RMSEP of the null model. *p* assesses whether using the current number of components is significantly different from using one component less. The degree of overall compression is assessed by linear regression of the cross-validated reconstructions on to the climate variable; b_1 and b_1.se are the slope and the standard error of the slope, respectively. The closer the slope (b_1) is to 1, the less the compression.

	n	R^2	Avg.bias	RMSEP	ΔRMSEP	*p*	b_1	b_1.se
MTCO (°C)	1	0.72	–1.11	6.83	–45.45	0.001	0.83	0.00
	2	0.74	–1.21	6.68	–2.25	0.001	0.84	0.00
	3	**0.75**	**–1.10**	**6.51**	**–2.48**	**0.001**	**0.85**	**0.00**
	4	0.75	–1.10	6.54	0.53	1.000	0.85	0.00
	5	0.75	–1.13	6.54	–0.07	0.188	0.85	0.00
MTWA (°C)	1	0.54	–0.33	3.89	–29.76	0.001	0.66	0.00
	2	0.58	–0.32	3.69	–5.10	0.001	0.71	0.00
	3	**0.59**	**–0.33**	**3.68**	**–0.14**	**0.001**	**0.71**	**0.00**
	4	0.59	–0.33	3.69	0.07	0.746	0.71	0.00
	5	0.59	–0.33	3.67	–0.39	0.001	0.71	0.00
α	1	0.62	–0.02	0.189	–37.73	0.001	0.66	0.00
	2	0.63	–0.022	0.188	–0.81	0.001	0.68	0.00
	3	0.63	–0.021	0.186	–0.87	0.001	0.68	0.00
	4	**0.65**	**–0.02**	**0.182**	**–2.11**	**0.001**	**0.71**	**0.00**
	5	0.65	–0.02	0.182	0.11	1.000	0.71	0.00

603 Table 3: Maximum likelihood estimates of the relationship between the change in mean
604 temperature of the coldest month (ΔMTCO) and the change in mean temperature of the
605 warmest month (ΔMTWA) by latitudinal bands for the northern extratropics (NET, north of
606 23.5°N), tropics (TROP, between 23.5°N and 23.5°S) and southern extratropics (SET, south of
607 23.5°S). The intercepts were set to zero since both variables are changes.

Region		Coefficient	Standard error (SE)	Lower 95%	Upper 95%
NET	Slope	2.183	0.334	1.528	2.838
TROP	Slope	1.427	0.509	0.430	2.425
SET	Slope	1.665	0.575	0.538	2.791

608

609

610 Table 4: Maximum likelihood estimates of the relationship between the change in plant-
611 available water (Δα) and the change in mean temperature of the warmest month (ΔMTWA) by
612 latitudinal bands for the northern extratropics (NET, north of 23.5°N), tropics (TROP, between
613 23.5°N and 23.5°S) and southern extratropics (SET, south of 23.5°S). The intercepts were set
614 to zero since both variables are changes.

Region		Coefficient	Standard error (SE)	Lower 95%	Upper 95%
NET	Slope	0.069	0.011	0.048	0.091
TROP	Slope	0.077	0.010	0.058	0.095
SET	Slope	0.054	0.014	0.027	0.082

615